# Nanoscale

Accepted Manuscript


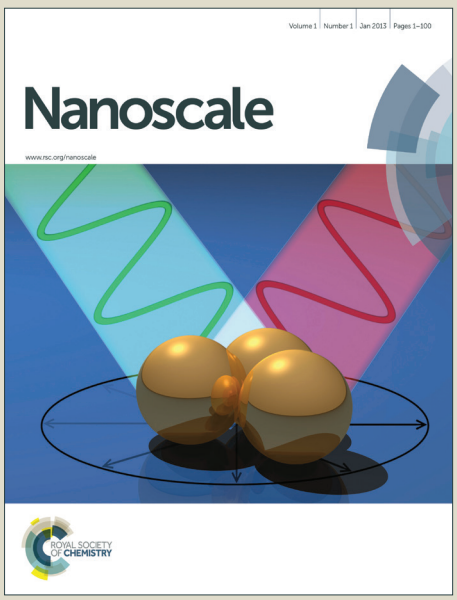





ROYAL SOCIETY OF CHEMISTRY

www.rsc.org/nanoscale

# Receptor-mediated Membrane Adhesion of Lipid-Polymer Hybrid (LPH) Nanoparticles Studied by Dissipative Particle Dynamics Simulations

*Zhenlong Li* and Alemayehu A. Gorfe**

Department of Integrative Biology and Pharmacology

The University of Texas Health Science Center at Houston, 6431 Fannin St., Houston, Texas 77030

*Email: zhenlong.li@uth.tmc.edu, alemayehu.a.gorfe@uth.tmc.edu

**Keywords:** Lipid-polymer hybrid (LPH) nanoparticle, targeted drug delivery, membrane adhesion, lipid bilayer, dissipative particle dynamics (DPD)

**Abstract**

Lipid-Polymer Hybrid (LPH) nanoparticles represent a novel class of targeted drug delivery platforms that combine the advantages of liposomes and biodegradable polymeric nanoparticles. However, the molecular details of the interaction between LPHs and their target cell membranes remain poorly understood. We have investigated the receptor-mediated membrane adhesion process of a ligand-tethered LPH nanoparticle using extensive Dissipative Particle Dynamics (DPD) simulations. We found that the spontaneous adhesion process follows a first-order kinetics characterized by two distinct stages: a rapid nanoparticle-membrane engagement followed by a slow growth in the number of ligand-receptor pairs coupled with structural re-organization of both the nanoparticle and the membrane. The number of ligand-receptor pairs increases with the dynamic segregation of ligands and receptors toward the adhesion zone and an out-of-plane deformation of the membrane. Moreover, fluidity of the lipid shell allows for strong nanoparticle-membrane interaction to occur even when the ligand density is low. LPH-membrane avidity is enhanced by the increased stability of each receptor-ligand pair due to the geometric confinement and cooperative effect arising from multiple binding events. Thus, our results reveal the unique advantages of LPH nanoparticles as active cell-targeting nanocarriers and provide some general principles governing

nanoparticle-cell interactions that may aid future design of LPHs with improved affinity and specificity for a given target of interest.

## 1. Introduction

Lipid-polymer hybrid (LPH) nanoparticles were first reported in 2008 as a class of promising next-generation nanoscale drug delivery platforms[1]. Despite continuous improvements in their synthesis, drug loading/release and cellular uptake profiles[1-7], the microscopic details of their interaction with cell membranes during active targeting remain elusive[7]. In this work, we have investigated the receptor-mediated membrane adhesion of a model LPH using Dissipative Particle Dynamics (DPD) simulations.

Adhesion of ligand-tethered nanoparticles onto receptor-bearing cell surfaces represents a critical step for the receptor-targeting nanoparticles to recognize and enter pathogenic cells[8, 9]. Understanding the molecular details of this process is necessary for the assessment of nanoparticle efficacy and structural optimization. Experimental techniques such as surface plasmon resonance (SPR) and fluorescence spectroscopy have been used to characterize the adhesion process *in vitro* by monitoring the adhesion and detachment events[10-14]. However, the limited resolution of these techniques does not allow for extracting individual adhesion events[10]. Another major challenge lies in the difficulty to predict the adhesion strength based on the ligand-receptor binding affinity due to lack of information on the equilibrium adhesion structure[12].

A variety of theoretical and computational models have been developed to interpret the mechanism of nanoparticle-membrane adhesion observed in macroscopic experimentations. For example, Ghaghada *et al* developed a mathematical model to characterize folate-tethered liposomes that target folate receptors[15]. Similarly, Decuzzi *et al* examined the active targeting of diseased microvasculature and proposed a number of geometrical and biological considerations that need to be taken into account during rational design of nanoparticles[16, 17]. Using multi-scale computations, Radharishnan and colleagues estimated the free energy landscape of nanoparticle adhesion onto endothelial cells[18-20] while Dormidotova and colleagues evaluated the influence of various nanoparticle surface structural parameters on the adhesion strength and specificity[21-23]. These studies provided a theoretical framework for optimizing nanoparticle

structure based on nanoparticle-cell interactions. Our focus here is to characterize the equilibrium adhesion mode of LPH nanoparticles.

Electron Microscopy (EM) and Dynamic Light Scattering (DLS) studies have shown that various LPH nanoparticles share a spherical core-shell-corona structure[1, 6] with the polymeric core, which consists of hydrophobic biodegradable polymers, functioning as the major drug reservoir. The core is covered by a lipid monolayer shell, in which a small fraction of lipids are covalently attached to the headgroup with hydrophilic polymers that form the corona. The distal end of the corona chain can be functionalized with targeting ligands that bind to specific cell-surface targets[1, 2]. Compared to traditional lipid-based or polymer-based nanoparticles, LPH nanoparticles have unique structural features that influence their interaction with cell membranes. For example, the lipid shell may facilitate re-organization of the polymer tethers and ligands on nanoparticle surface during adhesion. Furthermore, the core is an amorphous polymeric matrix that is less prone to deformation than the liquid interior of liposomes. These features make it difficult to directly apply generalized membrane adhesion models to LPH nanoparticles.

From a thermodynamic perspective, the system free energy of a nanoparticle-membrane assembly should decrease upon ligand-receptor association during adhesion[15, 24]. At the same time, ligand-receptor association introduces a restraint on the polymer tether ends and reduces the conformational freedom of the entire tether, which leads to entropic penalty. Furthermore, formation of multiple ligand-receptor interactions may also trigger membrane curvature[14]. The adhesion process is thus determined by the competition between these factors and involves a wide range of interactions. We chose DPD to circumvent the time and length-scale limitations associated with atomistic models. DPD is a mesoscopic particle-based simulation approach[25, 26] that has been widely used to study lipid membranes, membrane proteins and polymers[22, 27-29]. It allows for accurate modeling of hydrodynamic interactions and reproduces the static and dynamic properties of polymer chains in solution and melt[30, 31], and has been used to study receptor-mediated membrane adhesion of polymeric micelles[22] and cell-cell adhesion processes[28].

## 2. Method

In a DPD simulation, the system is coarse-grained into interacting beads and evolves based on Newton mechanics[25, 26]. A detailed description of the method and parameterization can be found in our previous publication[32].

Our model accounts for the molecular-level structure of the ligand-tethered LPH, the lipid membrane in which multiple trans-membrane receptors are embedded, and the solvent environment (Fig. 1). We used reduced DPD units for all variables, with particle mass $m_0$, diameter $d_0$ and time $t_0$ taken to be the mass, length and time unit, respectively. The pairwise conservative interaction parameters used for each pair are summarized in Table 1. The interaction parameter between W beads is $a_{WW}=25k_BT/d_0$. Together with an average number density of 3 for all beads, this ensures the ability to reproduce the compressibility of water at room temperature[26]. For the lipid molecules, the tail-water repulsive parameter ($a_{TlW}=75k_BT/d_0$) is made larger than that of headgroup-water ($a_{HlW}=35k_BT/d_0$), reflecting the amphiphilic nature of lipids. For the tether chains, the repulsive parameter with water ($a_{TeW}$) is the same as $a_{WW}$ as the chain is hydrophilic. For the core-forming chain, the repulsive parameter with water is larger than $a_{WW}$ to reflect the hydrophobic nature of the polymer.

**A. Model systems.** ***i) LPH nanoparticle:*** The LPH is made up of a core-forming polymer chain, unmodified lipids, and lipids with a hydrophilic polymer tether (Fig. 1a). Similar to our previous DPD study of lipid vesicles[33], a lipid molecule is modeled as a $H_4(T_4)_2$ amphiphile, where H is the hydrophilic headgroup and T is the hydrophobic tail (see Fig. 1a). Adjacent beads are connected by a harmonic potential $E_{l,b}=1/2k_{l,b}(r_{ij}-b_{l,b1})^2$ where $r_{ij}$ is the distance between two bonded beads. A force constant $k_{l,b}=100k_BT/d_0^2$ and equilibrium bond length $b_{l,b1}=d_0$ are used for all bonds except for the bond between bead 3 and 4, for which a shorter bond length $b_{l,b2}=0.8d_0$ is used. A harmonic potential $E_{l,a}=1/2k_{l,a}(\theta_l-\theta_{l,0})^2$ is applied to all bond angles $\theta_l$ with a force constant $k_{l,a}=40k_BT$ to maintain chain rigidity. The equilibrium angle $\theta_{l,0}$ is 120° for the bond angle between bead 2, 3 and 4, and 180° for all others.

Both the tether and core-forming chains are modeled as linear free-rotating chains (FRCs) (Fig. 1a). In each case intra-chain bonding interaction is modeled by a harmonic potential with a force constant $k_{p,b}=100k_BT$ and equilibrium bond length $b_{p,0}=1.0d_0$. The angle between two adjacent bonds ($\theta_p$) are restrained by a harmonic potential $E_{p,a}=1/2k_{angle}(\theta_p-\theta_{p,0})^2$ with a force constant $k_{p,a}=50k_BT$ and equilibrium bond angle $\theta_{p,0}=109.5^o$. The number of beads for the tether ($n_{tether}$) and the core ($n_{core}$) are 20 and 1000 respectively. One end of the tether is linked to a lipid headgroup (bead 1) using the same bond potential as that of the tether, while the distal end is modeled as a ligand bead (Lig) capable of forming reversible interaction with the active site of a membrane receptor (see below).

***ii) Lipid bilayer and receptor***: The lipid model for the bilayer membrane is the same as that of the nanoparticle shell (Fig. 1). Following a previous DPD study on cell-cell adhesion receptors[28], a receptor is modeled as a cylindrical trans-membrane protein (Fig. 1a). Specifically, the receptor molecule consists of 84 covalently linked beads evenly arranged in 12 layers along the bilayer normal. In each layer, the central bead is surrounded by 6 beads arranged in a hexagon of side $0.875d_0$. The distance between two neighboring layers is $0.8d_0$. These geometric parameters are maintained by harmonic bond and angle potentials ($k_{rb}=100k_BT$ and $k_{ra}=40k_BT$) applied on neighboring beads. The middle 6 layers are composed of hydrophobic beads ($TM_r$) and represent the trans-membrane segment. On each side of this segment are two layers of hydrophilic beads ($H_r$) that connect to a layer of hydrophilic beads ($A_r$) that bear the active site for ligand binding. The reason for the design of active sites on both ends is to enable binding of nanoparticle to either side of the membrane. The intra- and inter-molecular interaction parameters are set to $75k_BT/d_0$ for all receptor beads (Table 1) to maintain the cylindrical shape and prevent lateral self-aggregation.

***iii) Receptor-ligand interaction:*** Similar to a previous DPD study on the cell adhesion kinetics of ligand-tethered polymeric micelles[22], the reversible binding between a ligand and an active site of the receptor is modeled by the differential interactions of the ligand with the active site on the one hand and water on the other. Specifically, the repulsive interaction parameter between a ligand bead and an Ar bead ($a_{LigAr}$) is made smaller than $a_{LigW}$ so that the ligand has the tendency to associate with a proximal Ar bead. The

binding strength is tuned by the interaction parameter difference ($\Delta a = a_{LigW} - a_{LigAr}$), or simply $a_{LigAr}$ since $a_{LigW}$ is kept ($25k_BT/d_0$). Based on a previous survey of experimental ligand-receptor binding affinities[34], DPD study of micelle-membrane adhesion[22], and our test runs on the nanoparticle-membrane adhesion probability, we determined a series of binding strengths ($\Delta a$=19, 20, 22, $24k_BT/d_0$) that can lead to adhesion. To avoid simultaneous association of multiple ligands with the same receptor, a large self-repulsive parameter ($a_{LigLig}=75k_BT/d_0$) and cutoff distance ($r_c=2.0d_0$) were applied between ligand beads.

***iv)*** **Water:** Water molecules were represented by single beads (W).

**B. System setup and simulation protocol**

DPD simulations were conducted with the LAMMPS package[35] and analyzed with VMD[36]. The integration time interval $\Delta t$ was set to $0.02(m_0d_0^2/k_BT)^{1/2}$ for all simulations.

***i) Nanoparticle formation:*** The LPH nanoparticle was formed through self-assembly of model lipids and polymer chains in water. A core-forming polymer chain was first generated through self-avoiding random walk and placed at the center of a $30d_0 \times 30d_0 \times 30d_0$ simulation box. 600 lipid molecules were then randomly placed around the core-forming polymer chain. Among them, 10% (60) are covalently attached with a hydrophilic polymer chain and a ligand at the headgroup. This surface grafting density was based on previous experimental reports on the optimal range of nanoparticle surface grafting density for prolonged circulation time and limited toxicity[37]. The system was then solvated and simulated with periodic boundary condition at constant volume and temperature (NVT, $k_BT=1.0$) for 2,000,000 timesteps ($40{,}000t_0$). The coordinates were recorded every 100 timesteps ($2t_0$) for data analysis.

***ii) Ligand association with the soluble form of the receptor:*** To study the association stability of a receptor-ligand pair in the absence of the polymer tether and the trans-membrane segment of the receptor, we simulated the association of the soluble part of the receptor (i.e., the three layers including the active site and the linker) with the ligand using a larger force constant ($k_{ra}=100k_BT$) for all the bond angle potentials to maintain the cylindrical shape. All other parameters remained the same as the nanoparticle-membrane simulations. At each $\Delta a$, one soluble receptor and one ligand were placed in a water box of

$10d_0 \times 10d_0 \times 10d_0$ and simulated for $2\times10^7$ timesteps ($4\times10^5 t_0$), saving coordinates every 100 timesteps ($2t_0$).

***iii) Nanoparticle-membrane adhesion:*** A self-assembled bilayer of 288 lipids per leaflet from a previous study[33] was used as a starting point for the lipid membrane. After 25 receptors were evenly inserted, the bilayer was equilibrated for 1,000,000 timesteps ($20{,}000t_0$) at constant pressure and temperature (NPT, $P=23.88k_BT/d_0^3$, $k_BT=1.0$) condition to relax the bilayer to a nearly tensionless state (bilayer surface tension close to zero). The bilayer was then duplicated in a 2×2 grid and equilibrated, yielding a larger bilayer of 2306 lipids and 100 receptors. The final membrane area is $\sim1679.4d_0^2$, hence the average number density of the receptor is $\sim0.06d_0^{-2}$. To simulate the adhesion process, the membrane and the nanoparticle were placed in a $40.98d_0\times40.98d_0\times49.59d_0$ simulation box, with the bilayer normal being parallel to the z-axis. With PBC setting, the two surfaces of the bilayer were separated by the solvent with an average distance of $\sim43.3d_0$ along the z-axis. The nanoparticle was placed at the center of the solvent region so that its geometric center is equidistant ($\sim21.7d_0$) from the two surfaces of the membrane. This setup allows for the nanoparticle to be far away from each surface in the beginning and interacts with only one side at any given time. The system was equilibrated using NVT simulation for 10,000 timesteps ($200t_0$) applying position restraints along z-axis to both the membrane lipid headgroups and the nanoparticle core using a soft harmonic potential of force constant $k_m=5.0k_BT$. After equilibration, the position restraints were removed and NVT simulation was conducted for up to $1.2\times10^5 t_0$ to study the spontaneous adhesion process. For each $\Delta a$, 10 independent simulations were performed to improve sampling. Coordinates of the system were recorded every 1000 timesteps ($2t_0$) for data analysis.

## 3. Results and discussion

During the adhesion simulations, equilibration was monitored by the time evolution of the number of receptor-ligand pairs and the distance between LPH and membrane center of masses (Fig. 4, disused later). Both show that the spontaneous adhesion processes is completed at the time points indicated by the

second dashed lines in Fig. 4, and the system is stabilized thereafter. We used that part of the trajectory for analyses of equilibrium proprieties.

### *A. Equilibrium structure of the LPH nanoparticle.*

Visual inspection indicates that the LPH has a spherical core-shell-corona shape. The radial density profile of its constituents centered at the geometric center of the nanoparticle core (Fig. 2) shows that the polymeric core is about $4d_0$ in radius. The core includes part of the tail region from the lipid shell, which is a monolayer tightly packed lipids that protect the core from exposure to water. Based on the lipid headgroup distribution, the radius of the spherical shell is estimated to be $8.0d_0$. The corona is a dilute polymer brush tethered to the shell (Fig. 2b), with the distal end of the polymer extending to up to ~$16d_0$ from the nanoparticle center. The distribution of the tether length as measured by the end-to-end distance, $l_{tether}$, is Gaussian and can be described by (equ1):

$$P(\mathrm{l}_{\mathrm{tether}}) = \frac{1}{\sigma\sqrt{2\pi}} \exp\left(-\frac{\left(\mathrm{l}_{\mathrm{tether}} - l_{mean}\right)^2}{2\sigma^2}\right), \quad (1)$$

with an average length $l_{mean}$=$7.0d_0$ and standard deviation $\sigma$ =$2.2d_0$ (Fig. 2b, inset). Based on the chain statistics of FRCs[38], the root mean square end-to-end distance $\langle l_{tether}^2 \rangle^{1/2}$ can be calculated as (equ2):

$$\left\langle \mathrm{l}_{tether}^2 \right\rangle^{1/2} = \sqrt{n_{tether} b_{p,0}^2 \frac{1-\cos(\theta_{p,0})}{1+\cos(\theta_{p,0})}}, \quad (2)$$

which yields $6.3d_0$ using the tether bond number $n_{tether}$=20, equilibrium bond length $b_{p,0}$=$1.0d_0$ and bond angle $\theta_{p,0}$=120° (see Methods). This is slightly larger than $l_{mean}$ obtained from our simulation, indicating that the tethers are well solvated in the simulations.

### *B. Membrane adhesion is a two-stage process following first-order kinetics.*

In all nanoparticle-membrane adhesion simulations, the initial random motion of the nanoparticle in water triggers the formation of the first ligand-receptor contact, which is quickly followed by adherence to one

side of the membrane. This is illustrated in Fig. 3 using three representative snapshots for the initial, intermediate and final stages of a typical adhesion process for $\Delta a$=24$k_B$T. To quantitatively characterize this process, the average number of receptor-ligand contact *N(t)* and nanoparticle-membrane separation distance ($d_{nm}$) are monitored over time *t*. A ligand and a receptor are defined as bound to each other if the ligand is within a cutoff distance of 1.0$d_0$ from any $A_r$ bead of the receptor. $d_{nm}$ was calculated as the vertical distance between the nanoparticle center of geometry and its projection on the local bilayer mid-plane (defined by the average z position of lipid tail beads 8 and 12, see Fig. 3d). Fig. 4 shows the time-evolutions of *N(t)* and $d_{nm}$ for different $\Delta a$ values. For all $\Delta a$, the adhesion process can be divided into two stages based on the time it took for $d_{nm}$ to stabilize (Fig. 4, left dashed line). In the first stage, the nanoparticle is quickly pulled towards the bilayer leading to a sharp rise in *N(t)*. In the second stage, the nanoparticle maintains at a constant distance from the bilayer surface while *N*(*t*) rises at a lower rate. The slow increase of *N(t)* in the second phase can be attributed to the steric effect of the bound tethers and the reduced ligand concentration in the adhesion zone. More than half of ligand-receptor interactions are formed during this second stage.

For all simulations, the plots of *N*(*t*) can be fitted with a pseudo-first-order kinetics (equ3):

$$N(\mathrm{t}) = \mathrm{N_e}\left(1-\exp(-\mathrm{k}_{app}\mathrm{t})\right), \quad (3)$$

where *Ne* represents the equilibrium number of receptor-ligand contacts and $k_{app}$ is the apparent receptor-ligand association rate constant (Fig.4 and Table 2). This is consistent with the membrane adhesion kinetics of ligand-tethered polymeric micelles observed in a previous DPD study[22]. Although both *Ne* and $k_{app}$ increase with $\Delta a$ (table 2), the approximate time needed to reach equilibrium (Fig. 4, right dashed line) decreases with $\Delta a$, indicating that $k_{app}$ depends on $\Delta a$ more strongly than does *Ne*.

### *C. Lipid fluidity and tether extension enhance receptor-ligand interaction.*

The profile of *N(t)* and $d_{nm}$(Fig. 4) indicate that the simulations are well equilibrated within last 20,000$t_0$. Averaging over this portion of each trajectory yields an average $d_{nm}$ (<$d_{nm}$>) of 16.4$d_0$-17.4$d_0$ that only

slightly decreases with the increase of $\Delta a$ (Fig. 4 and table 2), whereas the average distance between the receptors active site and the bilayer mid-plane is ~4.0$d_0$. Combining with the nanoparticle lipid shell radius of ~8.0$d_0$ (see Fig. 2b and Fig. 3d), these yield 4.4$d_0$ for the minimal distance between the lipid shell surface and an active site facing the nanoparticle. Below we discuss the equilibrium structure of the nanoparticle and the membrane with the help of a simplified schematics of the relative position of the nanoparticle and the membrane displayed in Fig. 3d,

***i) Nanoparticle surface structural re-organization:*** It is expected that only ligands within certain distances from the membrane surface can bind to receptors, because the fixed tether length and nanoparticle-membrane separation distance would prevent some ligands from reaching the receptors. To characterize the distribution of receptor-bound ligands, we first calculated the number density profile of the ligand-tethered lipids (Fig. 5a) along the local bilayer normal (z-axis) (see Fig. 3d). We find that, for each $\Delta a$, the majority of the ligand-tethered lipids are on the side of the nanoparticle facing the membrane (Fig. 5b). In other words, the surface distribution of the ligand-tethered lipids is inhomogeneous and decreases sharply with the distance from the membrane surface. This suggests that LPH nanoparticles, similar to ligand-tethered liposomes[34], have the potential to enhance membrane adhesion by lateral re-organization of the lipid shell. Since the lateral diffusion of lipids in the lipid shell is influenced by the phase behavior of the lipid monolayer and the characteristics of the polymer tethers, these parameters can be tuned to facilitate the diffusion of tethered lipids towards the adhesion zone.

***ii)Tether extension:*** To determine the influence of membrane adhesion on the tether conformation, we calculated the average length $\langle l_{tether} \rangle$ of the liganded tethers as a function of the z-position of their fixed end (i. e., the lipid headgroup bead 1, see Fig. 5b and Fig. 3d). That $\langle l_{tether} \rangle$ is greater than $l_{mean}$ (see section A) indicates that the liganded tethers are under different levels of stress than the unliganded tethers; and the farther away these tethers are from the bilayer surface the larger their extension. This is consistent with a previous biophysical study that concluded that semi-flexible tethers become extended when bound to a surface through receptor-ligand association[24]. The linear correlation between $\langle l_{tether} \rangle$ and $z$, and hence the distance between the fixed ends and their projections on the bilayer surface, seems to

indicate that each ligand preferably binds to a receptor that faces its tether's fixed end. The maximal tether length (10.5-11.0$d_0$ at z = 0.0$d_0$) is determined by the upper limit of the tether length in the free state (section A, Fig. 2b inset) since, beyond $l_{mean}$ and until the tether reaches full extension, the entropic penalty is approximately proportional to[24] $<l_{mean}^2>$. As $d_{nm}$, the overall extension slightly decreases with $\Delta a$, and at larger $\Delta a$ more tethers bind receptors; hence on average each tether contributes less to the adhesion force to overcome the hydrodynamic drag force exerted by the solvent on the nanoparticle.

***iii) Receptor re-distribution:*** In Fig. 6a, the number density profiles for the ligand-bound and all receptors around the projection of the nanoparticle center on the membrane (see Fig. 3d) are plotted for all binding strengths. One can see that the ligand-bound receptors are almost evenly distributed under the projection of the nanoparticle shell ($R$<8.0$d_0$). Due to the restraint imposed by the tether length the density of the ligand-bound receptors decreases quickly after a distance equivalent to the maximum tether length, and the maximum extension is very similar for all $\Delta a$ since it is mainly determined by the extension limit of the tethers. The receptor density at the adhesion region is greater than that of the surrounding (Fig. 6a), indicating that adhesion induces receptor segregation.

***iv) Bilayer deformation:*** Fig. 3c suggests that the bilayer experienced out-of-plane deformation to accommodate the nanoparticle. We quantified this by calculating the average bilayer shape near the projection of the nanoparticle center (Fig. 6b) based on the average vertical displacement of the bilayer midplane ($\Delta h_z$) along the R axis using the nanoparticle projection as the starting point (see Fig. 3d). The result shows that the high surface curvature of the nanoparticle induces local curvature on the bilayer, and this effect increases with $\Delta a$ due to the tighter adhesion. Such negative membrane curvature may facilitate internalization of the nanoparticle. Conversely, one can surmise that membrane adhesion of nanoparticles may be facilitated by local negative membrane curvature[39].

Taken together, the equilibrium adhesion mode is affected by steric effects at the adhesion zone, lipid mobility, and the elastic properties of the polymer tethers and the membrane. While lateral diffusion of lipids and receptors is thermally excited and costs marginal energy, tether extension and membrane

bending would require expenditure of elastic energy. The balance between these factors, and the number of receptor-ligand interaction pairs, determines the equilibrium structure of the adhesion zone.

***D. Equilibrium dynamics of the nanoparticle-membrane adhesion.*** At equilibrium,*N(t)* remains constant (Fig. 4) despite fluctuation in the receptor-ligand interactions. To characterize this fluctuation in more detail, we used a time-dependent auto-correlation function *f(t)* that monitors the breaking of receptor-ligand interaction pairs. In this function, we record the total number of receptor-ligand pairs at time $t_{start}$ ($A(t_{start})$) and the identity of each ligand and receptor involved in the binding. We then record the number of surviving receptor-ligand pairs at subsequent time steps $t$ ($A(t)$), and calculate $f(t)$ as (equ 4):

$$f(\mathrm{t}) = \left\langle \frac{\mathrm{A(t)}}{A(\mathrm{t_{start}})} \right\rangle, \tag{4}$$

where <> denotes ensemble averaging over different $t_{start}$. This function records the total fraction of receptor-ligand pairs that break over time. Fig. 7a shows that $f(t)$ follows a first-order exponential decay at all binding strengths (equ 5 and Table 2):

$$f(\mathrm{t}) = 1 - \exp\left(\frac{t}{\tau}\right) \tag{5}$$

where the characteristic time $\tau$ can be interpreted as the average resident time of a receptor-ligand pair. Clearly, $\tau$ increases with $\Delta a$ since decay of *f(t)* slows down with $\Delta a$ (Fig. 7b).

For comparison, we also calculated the average resident time of a receptor-ligand pair in the absence of the confinement imposed by the membrane and the tether by simulating a single receptor-ligand pair in solution (see Methods) (Fig. 7b). Using the same distance criteria as in the complex nanoparticle-membrane system, the receptor and ligand pair in solution is defined to be in the bound state if they are within $1.0d_0$ of each other, and the average resident time is calculated by dividing the total time the pair spent in the bound state by the number of disassociation events during an extended time period. We found $\tau$ is larger in the membrane system for every $\Delta a$. The increase in the stability of the receptor-

ligand pairs in membrane can be understood from the decrease in the diffusion of receptor/ligand molecules and the co-operativity arising from the multivalent binding. The collective effect dampens the negative impact of the tether extension on the stability of receptor-ligand interactions.

The other dynamic feature of the adhesion process is lateral drift of the nanoparticle on the membrane surface[22], which we characterized based on the2-dimensional (2D) mean squared displacement (MSD) of the nanoparticle (Fig. 8). The linear fitting the MSD curves (Fig. 7b, $t > 500t_0$) yields the lateral diffusion coefficient $D_n$ via the Einstein equation. We found that though $D_n$ ($4.94\text{-}8.28\times10^{-4}d_0^2/t_0$, Table 2) decreases with the increase of $\Delta a$, in each case it is smaller by one and two orders of magnitude than the corresponding 2D diffusion coefficient of the unbound nanoparticle ($1.48\times10^{-3}d_0^2/t_0$) or receptor ($2.75\times10^{-3}d_0^2/t_0$)) in water and lipids ($1.58\times10^{-2}d_0^2/t_0$) in the bilayer, respectively. Clearly, lateral diffusion of the nanoparticle is significantly reduced by membrane adhesion, and is likely dependent on the dynamics of receptor-ligand binding plus the extent of the membrane's local negative curvature (Fig. 6d).

**4. Conclusion**

Motivated by the unique structure of self-assembled LPH nanoparticles and their potential as drug nanocarriers for active cell targeting[1, 3], we have studied the membrane adhesion of a model LPH nanoparticle mediated by multivalent receptor-ligand associations. We used DPD simulations that allowed us to model the spontaneous adhesion processes at the molecular level, accounting for such important factors as ligand-receptor binding strength, tether conformation, nanoparticle structural re-organization, receptor re-distribution, and membrane deformation. Major conclusions that have emerged from the simulations include the following. First, the adhesion process follows a pseudo-first-order kinetics (Fig. 4, table 2), similar to a previous observation on the membrane adhesion of ligand-tethered polymeric micelles[22]. Second, similar to ligand-tethered liposomes[34], lipid fluidity facilitates receptor-ligand association through the re-distribution of ligands on the nanoparticle surface while tether extension, receptor re-distribution and membrane deformation increase the number of receptor-ligand pairs. Thirdly, the nanoparticle-membrane system is at dynamic equilibrium involving multiple receptor-ligand

association/disassociation events (Fig. 7, 8). In short, multivalent binding and geometric confinement together enhance the stability of individual receptor-ligand pairs and overall avidity.

These results offer unique mechanistic insights into how ligand-tethered LPH nanoparticles bind to pathogenic cell membranes[1]. They also suggest that high affinity and specificity may be achieved even at relatively low tether grafting density, which is desirable to avoid excessively long *in vivo* circulation time after intravascular administration[8]. It is worth noting, however, that membrane adhesion of ligand-tethered nanoparticles is a function of multiple parameters, such as particle size, tether grafting density, tether length and flexibility, and the biophysical characteristics of the targeting systems[37]. Following adhesion, endocytosis of receptor-bound nanoparticles is a critical step for drug delivery. This process can also be studied by DPD simulations[40,41]. We are currently investigating the relative role of the various design parameters (discussed throughout this paper) on both targeting and engulfment in order to develop a set of rules that can guide efforts toward a systematic optimization of LPH nanoparticles.

**Acknowledgment**

This work is supported in part by a start-up fund from the University of Texas Medical School at Houston. We thank the Innovation for Cancer Prevention Research (ICPR) postdoctoral fellowship by the UThealth School of Public Health and Cancer Prevention and Research Institute of Texas (CPRIT, grant number: RP101503) for financial support, and the Texas Advanced Computing Center (TACC) for computational resources.

**Disclaimer**

The content is solely the responsibility of the authors and does not necessarily represent the official views of the funding agency.

**References**


1. L. Zhang, J. M. Chan, F. X. Gu, J.-W. Rhee, A. Z. Wang, A. F. Radovic-Moreno, F. Alexis, R. Langer and O. C. Farokhzad, *Acs Nano*, 2008, 2, 1696-1702.
2. C. Salvador-Morales, L. Zhang, R. Langer and O. C. Farokhzad, *Biomaterials*, 2009, 30, 2231-2240.
3. L. Zhang and L. Zhang, *Nano Life*, 2010, 1, 163-173.
4. C.-M. J. Hu, S. Kaushal, H. S. T. Cao, S. Aryal, M. Sartor, S. Esener, M. Bouvet and L. Zhang, *Mol. Pharm.*, 2010, 7, 914-920.
5. R. H. Fang, K. N. Chen, S. Aryal, C.-M. J. Hu, K. Zhang and L. Zhang, *Langmuir*, 2012, 28, 13824-13829.
6. Y. Kim, B. Lee Chung, M. Ma, W. J. Mulder, Z. A. Fayad, O. C. Farokhzad and R. Langer, *Nano Lett.*, 2012, 12, 3587-3591.
7. B. Mandal, H. Bhattacharjee, N. Mittal, H. Sah, P. Balabathula, L. A. Thoma and G. C. Wood, *Nanomed. Nanotechnol. Biol. Med.*, 2013, 9, 474-491.
8. J. D. Byrne, T. Betancourt and L. Brannon-Peppas, *Adv. Drug Delivery Rev.*, 2008, 60, 1615-1626.
9. D. Peer, J. M. Karp, S. Hong, O. C. Farokhzad, R. Margalit and R. Langer, *Nat. Nanotechnol.*, 2007, 2, 751-760.
10. J. B. Haun and D. A. Hammer, *Langmuir*, 2008, 24, 8821-8832.
11. A. Gunnarsson, L. Dexlin, P. Wallin, S. Svedhem, P. Jönsson, C. Wingren and F. Höök, *J. Am. Chem. Soc.* , 2011, 133, 14852-14855.
12. S. Hong, P. R. Leroueil, I. J. Majoros, B. G. Orr, J. R. Baker Jr and M. M. Banaszak Holl, *Chem. Biol.*, 2007, 14, 107-115.
13. C. Tassa, J. L. Duffner, T. A. Lewis, R. Weissleder, S. L. Schreiber, A. N. Koehler and S. Y. Shaw, *Bioconjugate Chem.*, 2009, 21, 14-19.
14. C. Wilhelm, F. Gazeau, J. Roger, J. Pons and J.-C. Bacri, *Langmuir*, 2002, 18, 8148-8155.
15. K. B. Ghaghada, J. Saul, J. V. Natarajan, R. V. Bellamkonda and A. V. Annapragada, *J. Controlled Release* 2005, 104, 113-128.
16. P. Decuzzi and M. Ferrari, *Biomaterials*, 2008, 29, 377-384.
17. P. Decuzzi, R. Pasqualini, W. Arap and M. Ferrari, *Pharm. Res.*, 2009, 26, 235-243.
18. N. J. Agrawal and R. Radhakrishnan, *J.Phys. Chem. C*, 2007, 111, 15848-15856.
19. J. Liu, G. E. Weller, B. Zern, P. S. Ayyaswamy, D. M. Eckmann, V. R. Muzykantov and R. Radhakrishnan, *Proc. Nat. Acad. Sci. U. S. A.*, 2010, 107, 16530-16535.

20. J. Liu, R. Bradley, D. M. Eckmann, P. S. Ayyaswamy and R. Radhakrishnan, *Current nanoscience*, 2011, 7, 727.
21. C.C. Chen and E. E. Dormidontova, *Langmuir*, 2005, 21, 5605-5615.
22. H. Djohari and E. E. Dormidontova, *Biomacromolecules*, 2009, 10, 3089-3097.
23. S. Wang and E. E. Dormidontova, *Phys. Rev. Lett.*, 2012, 109, 238102.
24. C. Jeppesen, J. Y. Wong, T. L. Kuhl, J. N. Israelachvili, N. Mullah, S. Zalipsky and C. M. Marques, *Science*, 2001, 293, 465-468.
25. P. Hoogerbrugge and J. Koelman, *Europhys. Lett.*, 1992, 19, 155.
26. R. D. Groot and P. B. Warren, *J. Chem. Phys.*, 1997, 107, 4423.
27. V. Ortiz, S. O. Nielsen, D. E. Discher, M. L. Klein, R. Lipowsky and J. Shillcock, *J. Phys. Chem. B,* 2005, 109, 17708-17714.
28. J. Hu, R. Lipowsky and T. R. Weikl, *Proc. Nat. Acad. Sci. U. S. A.*, 2013, 110, 15283-15288.
29. F. J.-M. De Meyer, M. Venturoli and B. Smit, *Biophys. J.*, 2008, 95, 1851-1865.
30. A. Schlijper, P. Hoogerbrugge and C. Manke, *J. Rheol.*, 1995, 39, 567-579.
31. N. Spenley, *Europhys. Lett.*, 2000, 49, 534.
32. Z. Li and E. E. Dormidontova, *Macromolecules*, 2010, 43, 3521-3531.
33. Z. Li, A. A. Gorfe, *J. Phys. Chem. B*, 2014, 30, 9028-9036.
34. N. W. Moore and T. L. Kuhl, *Biophys. J.*, 2006, 91, 1675-1687.
35. S. Plimpton, *J. Comput. Phys.*, 1995, 117, 1-19.
36. W. Humphrey, A. Dalke and K. Schulten, *J. Mol. Graphics* 1996, 14, 33-38.
37. B. Wang, C. V. Galliford and P. S. Low, *Nanomedicine*, 2014, 9, 313-330.
38. P. G. De Gennes, *Scaling concepts in polymer physics*, Cornell university press, 1979.
39. B. J. Reynwar, G. Illya, V. A. Harmandaris, M. M. Müller, K. Kremer and M. Deserno, *Nature*, 2007, 447, 461-464.
40. H. M. Ding, W. D. Tian and Y. Q. Ma, *ACS Nano,* 2012, 6, 1230-1238.
41. K. Yang, Y. Q. Ma, *Nat. Nanotechnol.* 2010, 5, 579-583.

# Tables

**Table 1. DPD conservative interaction parameters.**

| | $H_l$ | $T_l$ | W | Te | Lig | Co | $H_r$ | $TM_r$ | $A_r$ |
|---|---|---|---|---|---|---|---|---|---|
| **$H_l$** | 35 | 50 | 35 | 50 | 50 | 75 | 35 | 75 | 75 |
| **$T_l$** | | 20 | 75 | 75 | 75 | 27 | 50 | 24 | 75 |
| **W** | | | 25 | 25 | 25 | 75 | 35 | 75 | 75 |
| **Te** | | | | 25 | 25 | 75 | 35 | 75 | 75 |
| **Lig** | | | | | 75 | 75 | 25 | 75 | $a_{LigAr}$ |
| **Co** | | | | | | 25 | 75 | 75 | 75 |
| **$H_r$** | | | | | | | 75 | 75 | 75 |
| **$TM_r$** | | | | | | | | 75 | 75 |
| **$A_r$** | | | | | | | | | 75 |

$a_{LigAr}$ represents the receptor-ligand repulsive parameter that was varied (6, 5, 3, $1k_BT$) in different simulations to tune the receptor-ligand binding strength. $H_l$: lipid headgroup, $T_l$: lipid tail, W: water, Te: tether chain, Lig: ligand, Co: core-forming chain, $H_r$: hydrophilic linker of the receptor, $TM_r$: hydrophobic transmembrane segment of the receptor, $A_r$: active site of the receptor.

**Table 2 Summary of curve fitting results of Fig. 4 and 8.**

| $\Delta a/[k_BT]$ | $N_e$ | $k_{app}/[10^{-5}/t_0]$ | $<d_{nm}>/[d_0]$ | $D_n\ [10^{-4}d_0^2/t_0]$ |
|---|---|---|---|---|
| **19** | 8.0±0.3 | 5.1±0.8 | 17.4±0.3 | 8.28±0.02 |
| **20** | 11.9±0.2 | 5.1±0.4 | 17.2±0.3 | 7.36±0.02 |
| **22** | 19.5±0.3 | 7.5±0.5 | 16.7±0.2 | 5.45±0.02 |
| **24** | 26.8±0.3 | 8.7±0.5 | 16.4±0.2 | 4.94±0.01 |

$<d_{nm}>$ is the average vertical separation distance (see Fig. 3d) between the nanoparticle geometric center and the bilayer mid-plane at equilibrium. *Ne* and $k_{app}$ are fitting results of Fig. 4 using $N(t)=N_e(1-\exp(-k_{app}t))$. $D_n$ is fitting result of Fig. 8 (after $t = 500t_0$) using $MSD=4D_nt$.

# Figure captions

**Fig. 1 DPD models** (a) Models of the lipid, polymer chain, and receptor. The lipid headgroup beads (labeled 1-4) are in green and tail beads (5-12) are in cyan. For the polymer tether chain, the green bead and the yellow bead represent the lipid headgroup bead 1 and the ligand bead, respectively. Core (blue) represents the core-forming chain of the LPH nanoparticle. Note that the actual number of beads is 1000 for this chain. For the receptor, the active site is in light red, the linker in green and the trans-membrane segment in cyan. Molecules are not to scale. (b) Top and lateral side views of a lipid bilayer membrane containing 2306 lipids and 100 receptors. The color scheme is the same as in (a).

**Fig. 2 Equilibrium structure of the LPH nanoparticle.** (a) Snapshot of the equilibrium structure with the same color code as Fig. 1. (b) Radial number density profile of different beads centered on the nanoparticle geometric center; the tether profile includes the ligand beads. Inset: probability distribution of the end-to-end distance ($l_{tether}$) of the polymer tethers fitted with a Gaussian function.

**Fig. 3 Nanoparticle-membrane adhesion process.** Snapshots from the simulation with $\Delta a=24k_BT$ at (a) $t=0t_0$, (b) $t=20{,}000t_0$, and (c) $t=60{,}000t_0$. Color scheme is the same as Fig. 1 and water is not shown for

clarity. In b and c, receptor-bound ligands are highlighted in blue. (d) A schematic representation of the adhesion structure at equilibrium where $d_{nm}$ is the vertical separation distance between the nanoparticle and the membrane, $l_{tether}$ is the end-to-end distance of the polymer tethers. The Z-axis is along the bilayer normal with the geometric center of the nanoparticle as origin. R-axis is parallel to the bilayer plane with the projection of the nanoparticle center as the origin.

**Fig. 4 Time-evolution of *N(t)* and $l_{nm}$.** (a-d) represent plots for different binding strengths $\Delta a$=19 (a), 20 (b), 22 (c), and 24$k_BT$ (d). Both *N(t)* and $l_{nm}$ were averaged over 10 independent simulations. The blue line is fitting curve of *N(t)* and the dashed line indicates the average separation distance calculated using the last 20,000$t_0$ of $l_{nm}$.

**Fig. 5 Equilibrium structure of the nanoparticle surface on the membrane.** (a) Density profiles of all (dashed line) and receptor-bound (solid line) ligand and lipids on the nanoparticle surface along the bilayer normal (z-axis, see Fig. 3d for illustration). (b) Average end-to-end distance of the tethers as a function of the vertical distance between their fixed ends and the nanoparticle geometric center. Each curve was calculated using the last 20,000$t_0$ of adhesion simulations at different binding strengths ($\Delta a$=19, 20, 22, 24$k_BT$) and averaged over 10 independent simulations.

**Fig. 6 Equilibrium structure of the membrane.** (a) Radial number density profile of all (dashed line) and ligand-bound (solid lines) receptors around the nanoparticle projection on the bilayer (R-axis, see Fig. 3d for illustration). (b) The average displacement of the bilayer mid-plane relative to the projection of the nanoparticle geometric center on the bilayer mid-plane as a function of the R position. Data for different binding strengths ($\Delta a$=19, 20, 22, 24$k_BT$).

**Fig. 7 Equilibrium dynamics of the nanoparticle-membrane adhesion.** (a) Receptor-ligand disassociation *f(t)* and (b) average residence time. The membrane-bound state refers to the resident time obtained from fitting of the curves in (a) for different binding strengths ($\Delta a$=19, 20, 22, 24$k_BT$). The average resident time in solution was obtained from simulations of a single ligand and receptor pair (without the trans-membrane part) in water, and standard deviation was calculated using time block averaging.

**Fig. 8 MSD of the nanoparticle.** 2D Mean Squared Displacement (MSD) of the nanoparticle on the membrane. Dashed line indicates the starting time for linear fitting.

# Figures

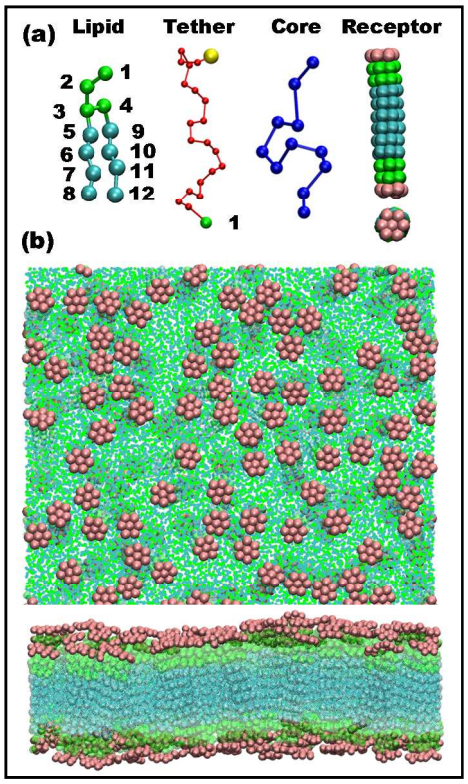


**Fig. 1**

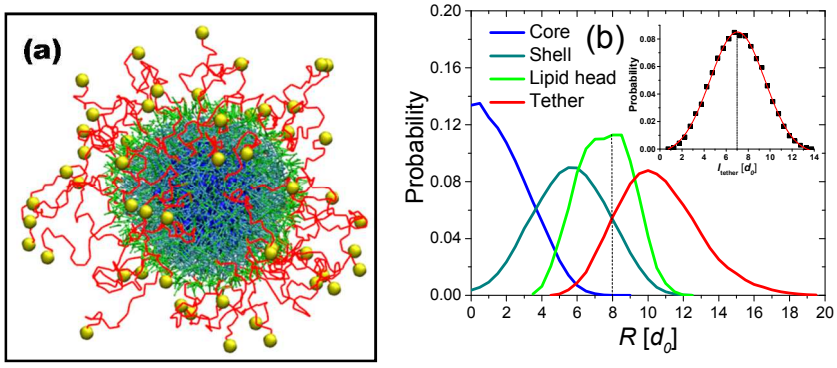


**Fig. 2**

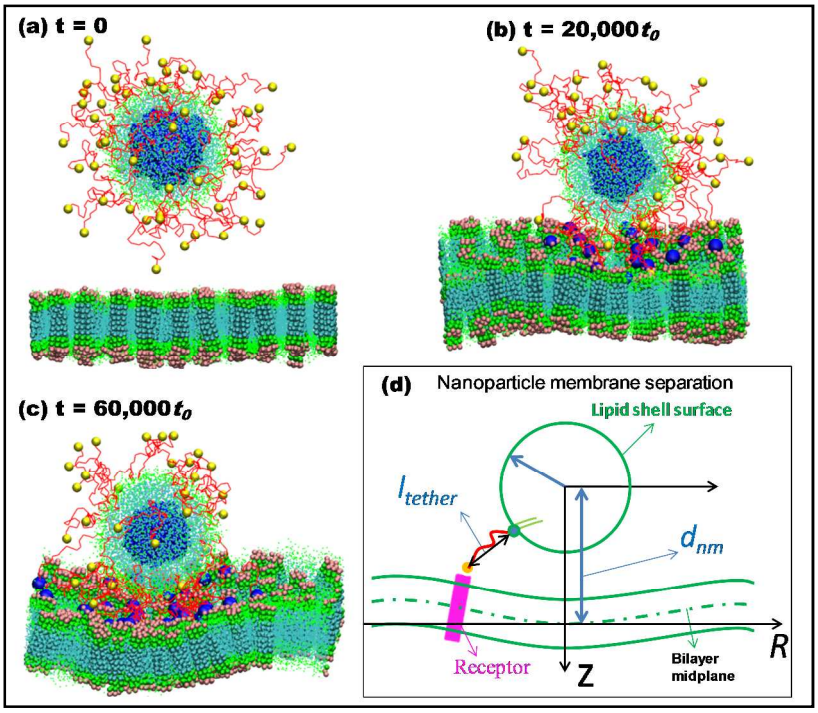


**Fig. 3**

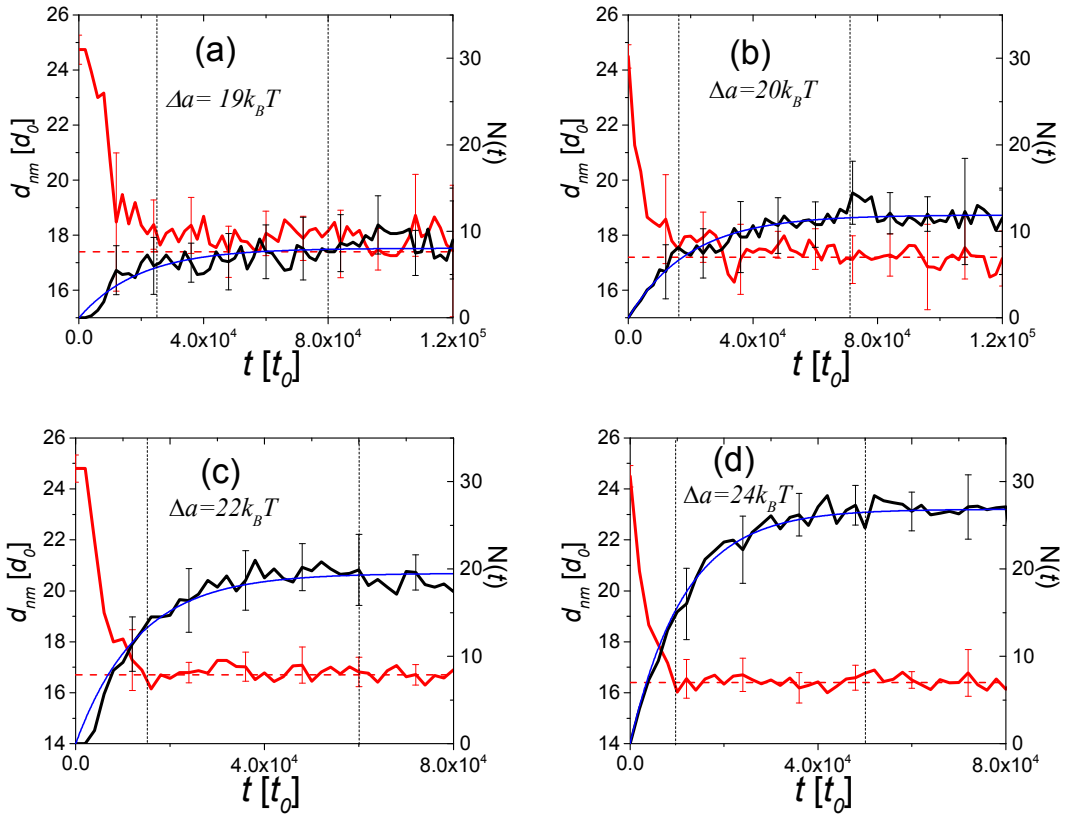


**Fig. 4**

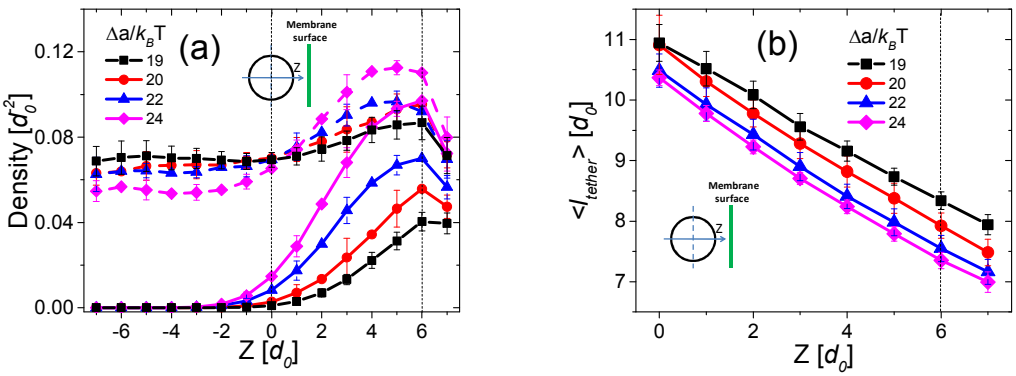


**Fig. 5**

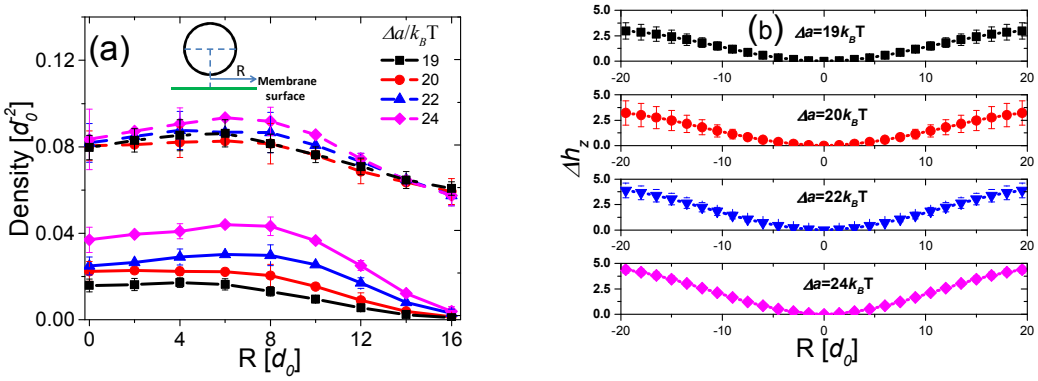


**Fig. 6**

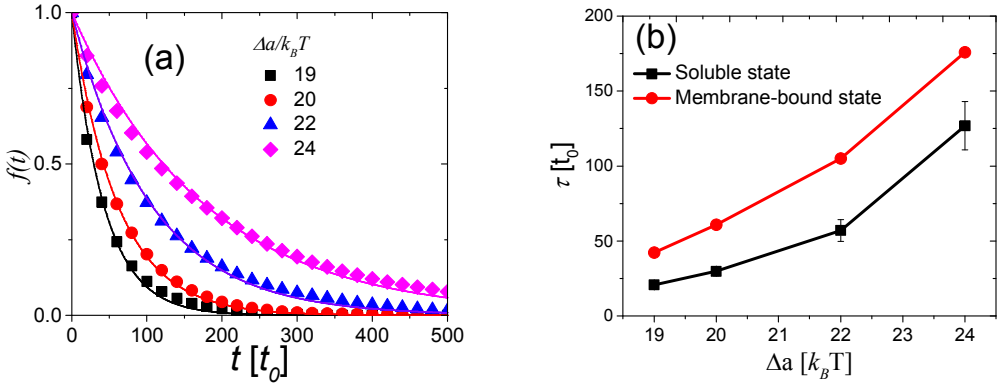


**Fig. 7**

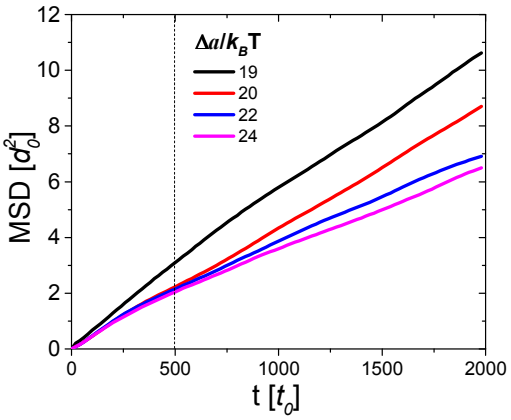


**Fig. 8**

TOC